Applied Catalysis A: General 384 (2010) 241–251

Contents lists available at ScienceDirect

Applied Catalysis A: General

journal homepage: www.elsevier.com/locate/apcata

Microstructure of leached Al-Cu-Fe quasicrystal with high catalytic performance for steam reforming of methanol

Toyokazu Tanabe[a,b,*], Satoshi Kameoka[a], An Pang Tsai[a,c]

[a] Institute of Multidisciplinary Research for Advanced Materials (IMRAM), Tohoku University, Sendai 980-8577, Japan
[b] Institute for Materials Research (IMR), Tohoku University, Sendai 980-8577, Japan
[c] National Institute of Materials Science (NIMS), Tsukuba 305-0047, Japan

ARTICLE INFO

Article history:
Received 2 April 2010
Received in revised form 19 June 2010
Accepted 21 June 2010
Available online 26 June 2010

Keywords:
Quasicrystal
Methanol steam reforming
Cross-sectional TEM
Cu catalyst
Raney catalyst

ABSTRACT

The catalytic performance of steam reforming of methanol (SRM), cross-sectional microstructure and leaching process of an $Al_{63}Cu_{25}Fe_{12}$ quasicrystal (QC) catalyst were studied. The QC catalyst was prepared by the NaOH leaching. The leaching of the QC alloy generated a homogeneous leached layer composed of Cu, Fe, Al, and their oxides. The activity and stability of the QC catalyst for the SRM was much superior to those of related crystalline alloy catalysts, because the highly dispersed Fe species in the homogeneous leached layer of the QC catalyst enhances the catalytic activity and suppresses the aggregation of Cu particles. The quasiperiodic structure of the Al-Cu-Fe QC was stable against leaching and had a relatively low dissolution rate of Al among the Al-Cu-Fe alloys, which resulted in the formation of a homogeneous leached layer that was responsible for the high activity and stability for SRM.

1. Introduction

Quasicrystals (QCs) are a unique form of matter that exhibit long-range order without periodicity and noncrystallographic rotational symmetries (i.e., 5-fold and 10-fold symmetries). Since they were first reported in 1984 by Shechtman et al. [1], over 100 binary, ternary, and quaternary alloy systems have been found to contain QC phases. Such systems possess extraordinary physical properties such as extremely high electrical resistance [2]. Interest in QCs as catalyst stems from the following unique properties that they offer: (1) brittleness, which allows them to be crushed to obtain fine particles; (2) a phase in thermodynamic equilibrium, which is stable at high temperatures; (3) a good composition, which includes a catalytic active element, such as Pd, Ni, or Cu; and (4) a unique surface structure, whose surface terminate as a QC bulk structure [3]. Because it is possible to develop unusual catalytic properties on the surfaces of QCs, the above-mentioned properties present an interesting area of study.

Hao et al. [4,5] have reported that a Ti-Zr-Co alloy containing an icosahedral QC phase showed high catalytic activity and selectivity for the oxidation of cyclohexane. However, Al-based QCs have been considered as one of the most promising candidates for a QC catalyst material because of thermal stability and ease of production. Surface studies have shown that the surface of Al-based QCs is covered with a thin Al oxide layer [6,7]. This layer is an obstacle when QCs are used as a catalyst material because the Al oxide is inactive. Pretreatment to remove the Al oxide (or Al) is thus necessary, and one available method involves a leaching treatment with alkaline solutions. This Al leaching process is the same as that which is applied to Raney catalysts which are made from Al-based alloys [8]. Tsai and Yoshimura [9,10] first employed leaching treatment in the preparation of catalysts from Al-based QC alloys. It has been reported that NaOH-leached Al-Cu-Fe QCs showed excellent activity for the steam reforming of methanol (SRM: $CH_3OH + H_2O \rightarrow 3H_2 + CO_2$). Its catalytic performance is as high as that of commercial Cu-based catalysts. Recently, several Al-based QCs (Al-Cu-Fe [11–13], Al-Cu-Ru [14], Al-Ni-Co [15]) have been applied to catalyst material by employing an alkali-leaching treatment. In these cases, the QC alloy is used as a precursor and/or a support. Although these reports suggest that the leached QC alloys show high catalytic performance and that the QC alloy is a good catalyst precursor, it is unclear as to how the QC works in the leaching process and catalytic activity.

A leached region composed of active metal nanoparticles is created by selectively dissolving Al from Al-based QC alloys by means of leaching. Although the leached region dominates the catalytic activity and stability of leached QC catalysts, no researcher has directly observed the leached region of the QC catalysts. The main problems in observing microstructure are presented by the deeply leached region that has a depth of more than several hundred nm

* Corresponding author at: Institute of Multidisciplinary Research for Advanced Materials (IMRAM), Tohoku University, 2-1-1 Katahira, Aoba-ku, Sendai 980-8577, Japan. Tel.: +81 0 22 217 5723; fax: +81 0 22 217 5723.
E-mail address: tanabe@tagen.tohoku.ac.jp (T. Tanabe).

0926-860X/$ – see front matter © 2010 Elsevier B.V. All rights reserved.
doi:10.1016/j.apcata.2010.06.045

depth [16]. Some studies of direct imaging for a Raney catalyst have been reported [17–20]. Smith et al. [17] have directly observed the porous Cu of a Raney Cu catalyst using a focused ion beam (FIB) miller and a transmission electron microscope (TEM). In this study, the preparation of the TEM samples was carried out by slicing the resin-embedded catalyst powder of an AlCuF QC catalyst, using Ar ion milling, then observing the cross-sectional microstructure with a TEM. Using a resin-embedded sample and Ar ion milling methods, the sample powder could be milled to the level of electron transparency (down to 100 nm thickness) while preserving it surface structure, thus allowing the direct observation of the cross-sectional structure of the QC catalyst particle.

Catalyst preparation conditions affect the structure and composition of the catalyst as well as its activity. Therefore, an understanding of the formation mechanism of the leached region of the leached alloy catalyst is highly desirable in order to obtain an optimal catalyst and precursor material. Study of the leaching kinetics of Raney Cu has showed that the mixed corrosion potential of the dissolving alloy is related to the leaching rate and that the formation mechanism of the Raney Cu structure mainly consists of the dissolution–redeposition of Cu atom [21,22]. This result suggests that the leaching rate (i.e., dissolution rate of Al from the precursor Al-based alloy) plays an important role in the formation mechanism of a leached alloy catalyst. To gain insight into the formation mechanism of QC catalysts, we examined an Al dissolution test for plate-type Al-Cu-Fe alloys in order to estimate the dissolution rate of Al from the precursor Al-Cu-Fe alloys.

This study aims (1) to test the catalytic activity and stability of Al-Cu-Fe QC and crystalline alloy catalysts prepared by alkali leaching for SRM; (2) to prepare a TEM sample using a resin-embedded sample and Ar ion milling methods and directly observe the cross-sectional microstructure of the leached region with a TEM; and (3) to examine the dissolution behavior of Al from Al-Cu-Fe alloys to clarify the formation mechanism of QC catalysts and the role of the QC structure. We will discuss the catalytic performance associated with the microstructure of the catalyst and the dissolution behavior of Al in the leaching process. We also show the role of the QC structure during leaching and how it assists in the determination of the microstructure that reveals the high catalytic performance of the SRM.

2. Experimental

2.1. Precursor alloy preparation

Two types of Al-Cu-Fe alloy (powder and plate) were prepared according to the method described below. Powder-type alloys were used as a catalyst precursor of the leached alloy catalyst and plate-type alloys were used for the dissolution test for Al under a leaching condition.

Al-Cu-Fe alloy ingots were prepared by melting mixtures of pure elements with purities of 99.9 wt% Al, 99.9 wt% Cu, and 99.9 wt% Fe in an argon atmosphere using an arc furnace. An annealing treatment for 24 h at each temperature under vacuum was applied to the as-cast ingots. The composition, annealing temperature, and structure of the precursor alloys are listed in Table 1. Powdered alloys were obtained by crushing and screening the annealed ingots to a particle size of 20–53 μm. Plate-type alloys were obtained by machining the annealed ingots to dimensions of 2 mm × 3 mm × 5 mm.

2.2. Catalyst preparation

Al-Cu-Fe alloy catalysts were prepared by alkali leaching of the powdered alloys, which were leached in a 5 wt% NaOH aqueous solution for 4 h at 296 K to remove the Al. The NaOH-leached powders were filtered out and thoroughly washed with distilled water until no alkali was detected in the filtrate. Finally, they were dried at 323 K overnight. The dissolution fractions of Al (=100 × amount of dissolved $Al_{(g)}$ into leaching solution/content of $Al_{(g)}$ in precursor alloy) were analyzed with an ICP spectrophotometer (PerkinElmer, Optima 3300). The dissolution test for Al was examined by alkali leaching of the plate-type alloys, which were leached with 5 wt% NaOH aq. at 343 K for 2 h. The apparent dissolution rates of Al for the Al-Cu-Fe alloys were estimated by analyzing the total dissolved Al in the initial stage of leaching in successive samples with the ICP.

A Cu/ZnO catalyst (Cu:Zn = 3:7 mol ratio) was prepared by a conventional coprecipitation method [23]. 200 cm^3 of a mixed aqueous solution of copper and zinc nitrate with a total concentration of 1.0 mol/l and 200 cm^3 of an aqueous solution of sodium carbonate (1.0 mol/l) were simultaneously added dropwise to 400 cm^3 of distilled water over 40 min while being stirred at room temperature. The formed precipitates were then aged at room temperature for 48 h while being stirred, and were then filtered, washed with distilled water, dried at 393 K overnight, and calcined at 623 K for 3 h in air.

2.3. Characterization of catalyst

Using a surface area analyzer (BEL Japan, Belsorp-mini), specific BET surface areas of the catalyst particles were determined by their N_2 adsorption at 77 K. The specific Cu surface areas of the catalyst samples were measured by nitrous oxide (N_2O) chemisorptions, using a method based on a procedure reported by Evans et al. [24]. The Cu surface areas were calculated from the amount of N_2O consumption at 363 K: $N_2O + 2Cu_s \rightarrow Cu_s\text{–}O\text{–}Cu_s + N_2$ where Cu_s is a surface Cu atom. Prior to the N_2O chemisorptions, each catalyst was reduced in 5% H_2/Ar for 1 h at 523 K in a conventional flow reactor. A copper atomic density of 1.46×10^{19} atom/m^2 was used to calculate the specific Cu surface area. The bulk structures of each sample were identified by means of X-ray diffraction (Rigaku, RINT 2500). The X-ray source was Cu Kα (λ = 1.543 Å) operating at 40 kV and 30 mA. The Scherrer equation was applied to the Cu (2 0 0) diffraction peak at $2\theta = 50.4^\circ$ in order to calculate the size of the Cu crystallite. The surface and fracture morphologies of the leached alloys were observed with a scanning electron microscope (SEM) (Zeiss, LEO 982) and their compositions were analyzed by an energy-dispersive X-ray spectroscope (EDS) that was attached onto the SEM.

2.4. Cross-sectional observation with TEM

TEM specimens for cross-sectional observation were prepared by a method that employed resin-embedding and Ar ion milling. The catalyst powders were mixed with resins (Koyo chemicals, KPR-30) and dropped onto a Mo mesh. After thermosetting at 353 K for 4 h, the resins were thinned with an Ar ion miller (BAL-TEC, RES 010 and JEOL, EM-09100IS). TEM analysis was carried out with a JEOL 2010 microscope with an operating voltage of 200 kV. The composition of the catalyst powders was analyzed by an EDS spectrometer, which is an Oxford link system that which was attached onto the TEM.

2.5. Steam reforming of methanol (SRM) reaction

The SRM experiments were carried out in a conventional flow reactor at atmospheric pressure. All the catalysts were pretreated in the flow reactor with 50% H_2/N_2 at 573 K for 20 min. The standard reaction conditions were 32% of methanol, 48% of H_2O, and N_2 (balance) at a liquid hourly space velocity of 60–70 h^{-1} (CH_3OH/H_2O = 2/3 mol ratio) with a catalyst bed weight of 0.2 g.

Table 1
Composition, annealing temperature, structure of precursor Al-Cu-Fe alloys and leaching properties (dissolution fraction of Al, BET surface area of leached alloy).

Sample	Precursor alloy						Dissolution fraction of Al[c] (%)	S_{BET}[d] (m^2/g_{cat})
	Type	Composition (at.%)			Annealing temp. (K)	Phase (structure)		
		Al	Cu	Fe				
QC-AlCuFe	Powder[a]	63	25	12	1073	QC(Quasicrystal)	58	20
C- AlCuFe	Powder[a]	70	20	10	973	ω(Tetragonal)	93	28
C- AlCu	Powder[a]	67	33		893	θ(Tetragonal)	89	31
C- AlFe	Powder[a]	76		24	1123	λ(Monoclinic)	94	46
QC-AlCuFe(plate)	Plate[b]	63	25	12	1073	QC(Quasicrystal)	–	–
C-AlCuFe(plate)	Plate[b]	70	20	10	973	ω(Tetragonal)	–	–
C-AlCu(plate)	Plate[b]	67	33		893	θ(Tetragonal)	–	–
C-AlFe(plate)	Plate[b]	66.5		33.5	1173	Al_2Fe(Triclinic)	–	–
C-AlCuFe-b(plate)	Plate[b]	52	32	16	1173	β(Cubic)	–	–

[a] Particle size of 20–53 μm.
[b] Dimension of 2 mm × 3 mm × 5 mm.
[c] Dissolution fraction of Al (=100 × amount of dissolved $Al_{(g)}$ into leaching solution/content of Al $_{(g)}$ in precursor alloy).
[d] BET surface area.

The gas products after water trapping were monitored by an on-line gas chromatograph (TCD) (Shimadzu, GC-14B). The data in the catalytic activity measurements were recorded when the reaction reached a steady state after 30 min at each reaction temperature. The catalytic activities of the SRM were evaluated by the rate of H_2 production per surface area ($mol/s/m_{cat}^2$) and the H_2 production activity in terms of the turnover frequency (TOF) (i.e., number of H_2 molecules produced per surface Cu atom per second). The number of surface atoms was calculated for the Cu surface area using a mean surface atom density of 1.46×10^{19} atom/m^2 [24]. Time-on-stream tests to investigate the catalyst stability for SRM were carried out in the following manner. The reaction temperature was raised to 593 K at a heating rate of 2 K/min. After the temperature reached at final set point of 593 K, it was kept constant for ca. 50 h; gas analysis was carried out at moderate intervals during this period.

3. Results and discussion

3.1. Leaching treatment

Fig. 1 shows powder X-ray diffraction patterns (XRD) for the powdered Al-Cu-Fe alloys before and after leaching treatment with NaOH solution. Before leaching (Fig. 1(a)), all the precursor alloy powders consisted mostly of a single phase: Icosahedral quasicrystalline (QC) phase ($Al_{63}Cu_{25}Fe_{12}$) [25], ω phase ($Al_{70}Cu_{20}Fe_{10}$) [PDF#25-1121], θ phase ($Al_{67}Cu_{33}$) [PDF#25-0012], or λ phase ($Al_{76}Fe_{24}$) [PDF#38-1147]. After leaching treatment (Fig. 1(b)), Cu, Cu_2O, and Fe_3O_4 appeared in the diffraction patterns. It is clear that the diffraction peaks of the crystalline phases (i.e., θ, ω, and λ phases) completely disappeared during the leaching treatment, whereas those of the QC phase persisted in the leached sample. The leaching treatment resulted in the highly selective removal of Al from the original Al-Cu-Fe alloys. In all the leaching solutions, no Cu and Fe was detected by ICP analysis. The dissolution fractions of Al from the precursor alloys are also listed in Table 1. Upon leaching, most of the Al (>90%) in the crystalline phases dissolves into the leaching solutions, but an adequate amount of Al remains in the QC phase. This result indicates that the QC phase is relatively more stable against alkali leaching than the crystalline phases with similar composition. The leached alloy catalysts were denoted according to their precursor alloy structure and constituent element. Thus, the leached catalyst prepared from QC Al-Cu-Fe alloy ($Al_{63}Cu_{25}Fe_{12}$) is written as QC-AlCuFe and the catalyst prepared from crystalline Al-Cu-Fe alloy ($Al_{70}Cu_{20}Fe_{10}$) is written as C-AlCuFe as listed in Table 1.

3.2. Catalytic activity and stability of SRM

Prior to the SRM reaction, a pretreatment with 50% H_2/N_2 at 573 K for 20 min was carried out for all the catalysts in order to reduce the Cu oxides. In all the reactions, the product gas contained H_2 and CO_2 as its major components, together with a small amount of CO (<0.3 vol%). No other products, such as dimethyl ether, methyl formate, or methane, were detected. Fig. 2(a) shows the production rates of H_2 per surface area as a function of the reaction temperature for the initial activities and the result of a conventional Cu/ZnO catalyst are also shown for comparison. The leached Al-Cu-Fe alloy catalysts exhibited catalytic activity for the SRM, except for the Al-Fe alloy catalyst (C-AlFe). This suggests that the catalytic activities are attributed to a copper species generated by the leaching treatment. Among the catalysts, the highest H_2 production rate based on surface area was obtained for QC-AlCuFe. The Arrhenius plots, as shown in Fig. 2(b), exhibited a good linearity. The apparent activation energy was calculated, and the results are listed in Table 2. No significant difference in activation energy was observed among the leached Al-Cu-Fe alloy catalysts. This indicates that the reaction mechanism of the SRM does not change for different catalysts. The characteristics of the catalytic activity for the SRM are summarized

Table 2
Characteristics of initial activity for SRM of Al-Cu-Fe alloy catalysts and Cu/ZnO catalyst.

Sample	E_a (kJ/mol)	H_2 production rate per catalyst weight[b] (μmol $H_2/s/g_{cat}$)	Cu surface area[c] (m^2/g_{cat})	TOF[d] (s^{-1})
QC-AlCuFe	46	306.9	9.7	1.31
C-AlCuFe	48	374.5	14.2	1.09
C-AlCu	47	317.4	13.6	0.96
Cu/ZnO[a]	34	372.2	21.7	0.71

[a] Prepared by coprecipitation method (Cu:Zn = 3:7 mol ratio, S_{BET} = 57 m^2/g_{cat}).
[b] Reaction temperature at 573 K.
[c] Determined by N_2O chemisorptions at 363 K (a copper atomic density of 1.46×10^{19} atom/m^2 was used to calculate the Cu surface are).
[d] H_2 molecules produced per surface copper atom per second (reaction temperature at 573 K).

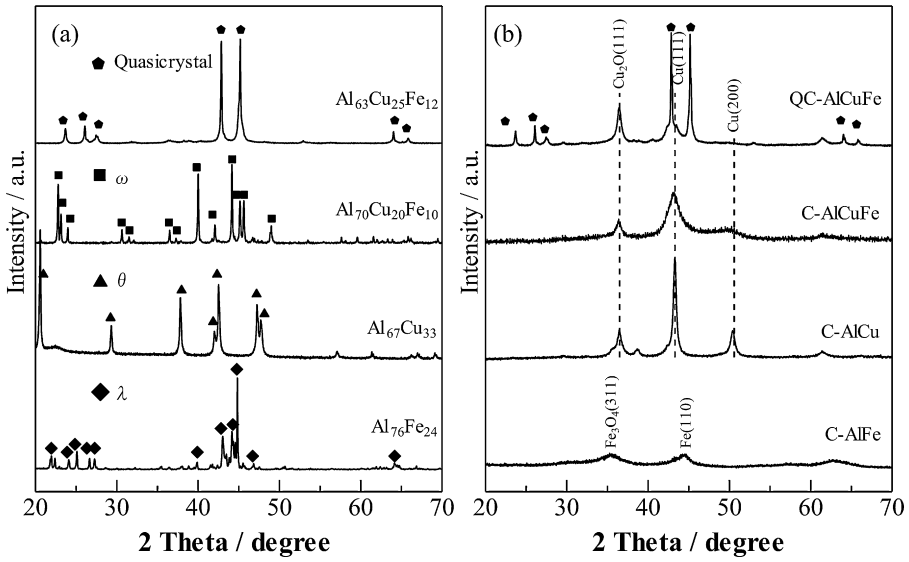

Fig. 1. Powder X-ray diffraction patterns for the Al-Cu-Fe alloys before (a) and after leaching treatment (b).

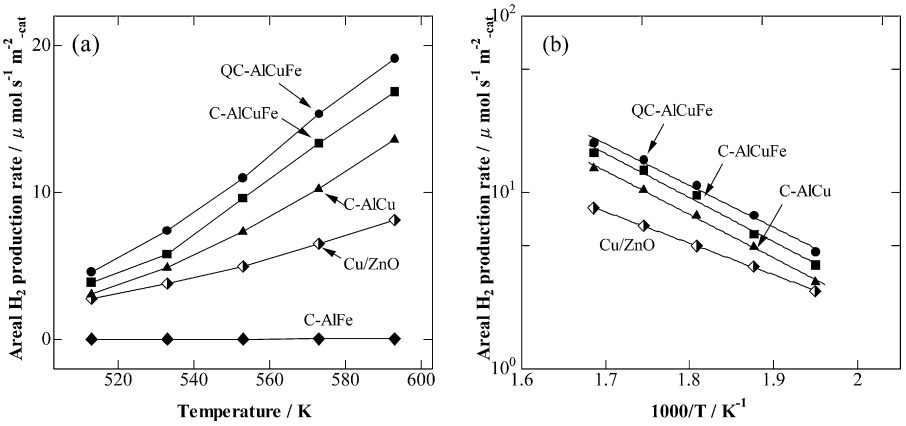

Fig. 2. Areal H_2 production rates of Al-Cu-Fe alloy catalysts for initial activities of SRM as a function of reaction temperature (a) and Arrhenius plots (b).

in Table 2. Although QC-AlCuFe exhibited the lowest values for the production rate of H_2 per catalyst weight and Cu surface area, owing to the incomplete leaching of the precursor QC alloy (Fig. 1(b)), the highest TOF value was obtained for QC-AlCuFe. It was found that the active Cu species fabricated from the QC alloy by leaching showed a higher level of activity than those prepared from the crystalline phases.

One important issue in use of a Cu-based catalyst for SRM is deactivation in the course of time [26]. Fig. 3 shows methanol conversions as a function of time on-stream at 593 K. QC-AlCuFe showed the best stability among the alloy catalysts, with its original activity decayed by 13% after 50 h on-stream. Its stability was comparable to that of the Cu/ZnO catalyst. On the other hand, severe deactivation occurred for C-AlCuFe and C-AlCu, with a loss of activity of 66% and 54%, respectively, during the same period. QC-AlCuFe reached a constant activity, while C-AlCuFe and C-AlCu seemed to deactivate and did not function as stable catalysts under the SRM condition. The QC catalyst showed higher durability than crystalline catalyst. Cu-based catalysts are susceptible to thermal sintering via a surface migration due to their relatively low melting points. Active Cu nanoparticles generally sinter at temperatures higher than 573 K for Cu-based catalysts [26]. Fig. 4 shows the powder XRD patterns for both the fresh (after H_2 pretreatment) and spent (after time-on-stream) catalysts. The fresh catalysts (Fig. 4(a)) showed that the Cu oxides generated by leaching were reduced

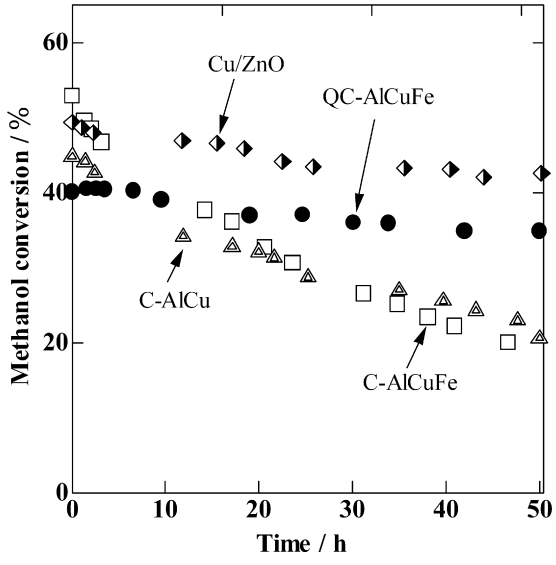

Fig. 3. Methanol conversions as a function of time-on-stream at 593 K for SRM over Al-Cu-Fe alloy catalysts and Cu/ZnO catalyst.

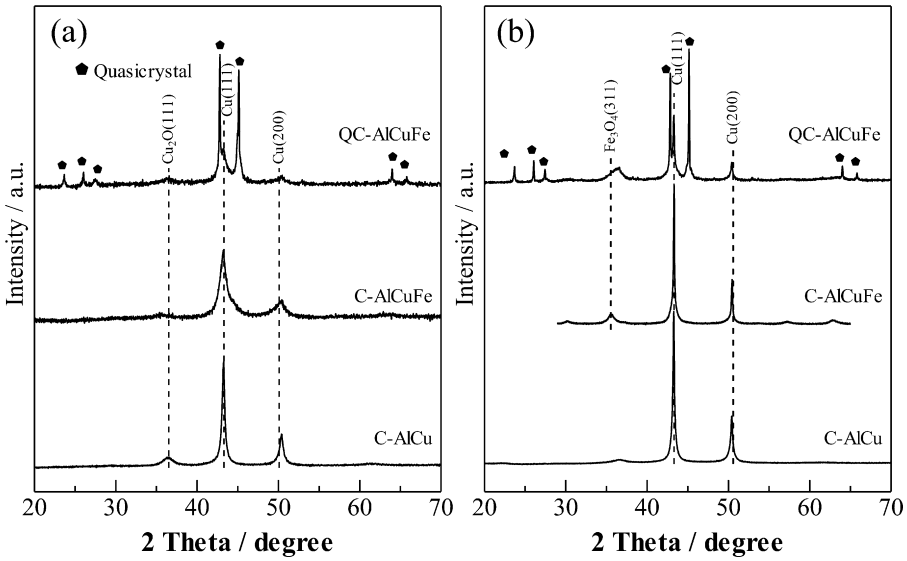

Fig. 4. Powder X-ray diffraction patterns for (a) fresh (after H_2 pretreatment with 50% H_2/N_2 at 573 K for 20 min) and (b) spent (after time-on-stream for SRM at 593 K for 50 h) catalysts of Al-Cu-Fe alloy catalysts.

with the H_2 pretreatment prior to the SRM reaction. After the time on-stream experiment (Fig. 4(b)), a sharpening of the diffraction peaks of Cu was observed in all the spent catalysts. The Cu crystallite sizes, as estimated from the half widths of the Cu (2 0 0) peaks using the Scherrer equation, are shown in Table 3. The Cu crystallite sizes of QC-AlCuFe increased slightly after the reaction. However, C-AlCuFe and C-AlCu, which exhibited rapid deactivation in the time course experiments, showed drastic increases in Cu crystallite sizes. These results indicate that the main contribution to the deactivation of the SRM is the sintering of Cu.

3.3. Cross-sectional observation with TEM

Fig. 5 shows SEM images of fresh QC-AlCuFe and C-AlCuFe. These images show that the particle sizes of the Cu on the surface were of the same dimension (ca. 10–20 nm) among the Al-Cu-Fe alloy catalysts. There was a clear difference, however, in cross-sectional structure between the two catalysts, as verified by direct observation with TEM. Fig. 6(a and b) shows cross-sectional TEM bright-field images of fresh QC-AlCuFe. It is clear that a leached layer about 500 nm thick was generated at the outer layer of the QC-AlCuFe particle. Selected area electron diffraction (SAED) patterns (Fig. 6(c)), line profiles of the SAED (Fig. 6(d)), and EDS spectra (Fig. 6(e)) are also shown in Fig. 6. The SAED patterns and EDS spectra (1–3) were obtained from regions 1–3, respectively, in Fig. 6(b). The line profiles of the SAED obtained from the leached layer (regions 1 and 2) could be assigned to Cu, Cu_2O, and Fe_3O_4. Composition analysis performed with an EDS showed that regions 1 and 2 were composed mainly of Cu, Fe, O, and a small amount of Al. It should be noted that both the regions (1 and 2) showed similar EDS spectra, indicating they have almost same composition. The leached regions generated in QC-AlCuFe had uniform composition and consisted of the homogeneous mixture of Cu, Fe, Al, and their oxides. The SAED pattern of the region 3 in the inner area of the QC-AlCuFe particle showed a 2-fold symmetry of reflections with quasiperiodicity, which characterizes the structure of QC. This observation confirmed that the QC persists in the inner area of the catalyst particles even after leaching.

Table 3
Cu crystallite size of fresh and spent catalyst of Al-Cu-Fe alloy catalysts.

Sample	Cu crystallite size[a] (nm)	
	Fresh[b]	Spent[c]
QC-AlCuFe	21	27
C-AlCuFe	17	68
C-AlCu	27	43

[a] The crystallite size was obtained for Cu (200) peak of XRD by Scherrer equation.
[b] After H_2 pretreatment in 50% H_2/N_2 at 573 K for 20 min.
[c] After time-on-stream experiment for SRM at 593 K for 50 h.

Fig. 7(a and b) shows cross-sectional TEM bright-field images of fresh C-AlCuFe. As shown in Fig. 7(a), the original crystalline Al-Cu-Fe alloy completely disappeared during the leaching process, and a complicated leached layer was formed in its place. It should be noted that a uniform contrast area about 100 nm thick was observed at the edge of the C-AlCuFe particle, whose area is assigned to region 1 in Fig. 7(b). The line profile of the SAED (Fig. 7(d)) obtained from the edge (region 1) could be assigned to Cu and Cu_2O, and composition analysis (Fig. 7(e)) verified that the edge is mainly composed of Cu and includes a minute amount of Fe and Al. The line profiles of the SAED and EDS spectra taken from regions 2 and 3 in the inner area, however, indicated that the inner area consists of a fine dispersion of Cu, Fe, Al, and their oxides. The microstructure of the inner area (regions 2 and 3) is quite different from that of the edge (region 1). Obviously, the leaching of the crystalline Al-Cu-Fe alloy ($Al_{70}Cu_{20}Fe_{10}$) gives rise to the enrichment of Cu (Cu-layer) at the edge of the catalyst particle.

Fig. 8(a and b) shows cross-sectional TEM bright-field images of spent QC-AlCuFe and C-AlCuFe, respectively. The SAED patterns obtained from the circled region in the figures are also shown. Spent QC-AlCuFe (Fig. 8(a)) showed no visible change in microstructure or SAED pattern compared to fresh catalyst (Fig. 6(b and c)). This observation suggests that the homogeneous leached layer of QC-AlCuFe has high stability under the SRM reaction. Clearly, the lower degree of degradation in the activity of QC-AlCuFe (Fig. 3) is due to the stability of the homogenous layer. On the other hand, for spent C-AlCuFe (Fig. 8(b)), the SAED shows a large single crystal region of Cu at the edge, whose area is identical to that of the Cu-enrichment (Cu-layer) in fresh C-AlCuFe (Fig. 7(b)). This conclusively shows a visible crystal growth of Cu, i.e., the sintering of Cu particles developed in the Cu-layer during the SRM, which leads to the degradation of the activity of C-AlCuFe upon the SRM (Fig. 3).

The cross-sectional observations with the TEM provided clear evidence that the microstructure of the leached layer is strongly

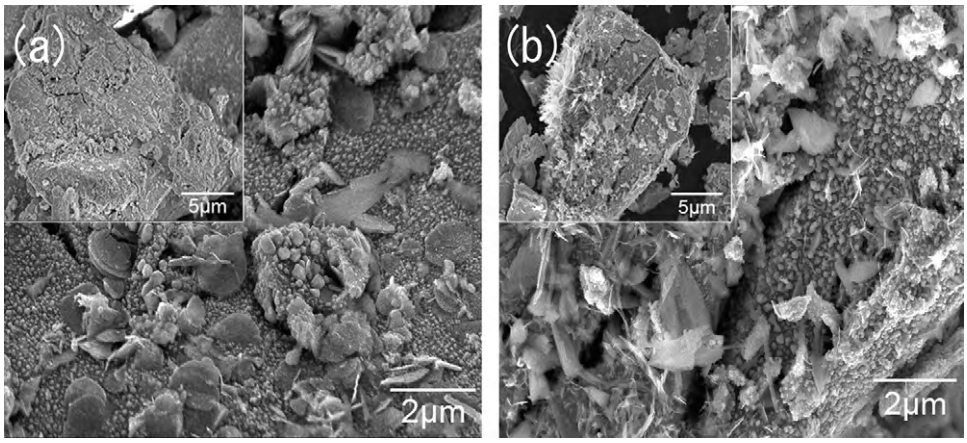

Fig. 5. SEM images for quasicrystalline $Al_{63}Cu_{25}Fe_{12}$ alloy catalyst (QC-AlCuFe) (a) and crystalline $Al_{70}Cu_{20}Fe_{10}$ alloy catalyst (C-AlCuFe) (b).

dominated by the precursor alloy. Since catalytic reaction proceeds on the surface of a catalyst particle, the leached layers are responsible for the catalytic performance. QC-AlCuFe has a more homogeneous leached layer than C-AlCuFe. Therefore, the formation of the homogeneous leached layer would be attributed to the high catalytic performance for SRM of QC-AlCuFe. We would propose that Fe species in the leached layer plays an important role in the high catalytic performance of QC-AlCuFe. Fe species offers two beneficial effects for the enhancement of catalytic activity and stability. One is the inhibition of the sintering of Cu due to the immiscible relationship between Cu and Fe. According to the binary phase diagram [27], Fe is immiscible with Cu, i.e., they neither form compounds nor mutually dissolves in solid state. In other words, Cu atoms cannot move through regions of Fe or Fe oxide; hence, the existence of Fe or Fe oxides around the Cu particles would block the path of diffusion of Cu atoms at elevated temperatures. This assertion has been verified by several observations [28–30]. Kawamura et al. [28] have reported that the addition of Fe to $Cu/ZnO/Al_2O_3$ contributes significantly to the suppression of the reduction of Cu surface area. Yahiro et al. [29] have reported that

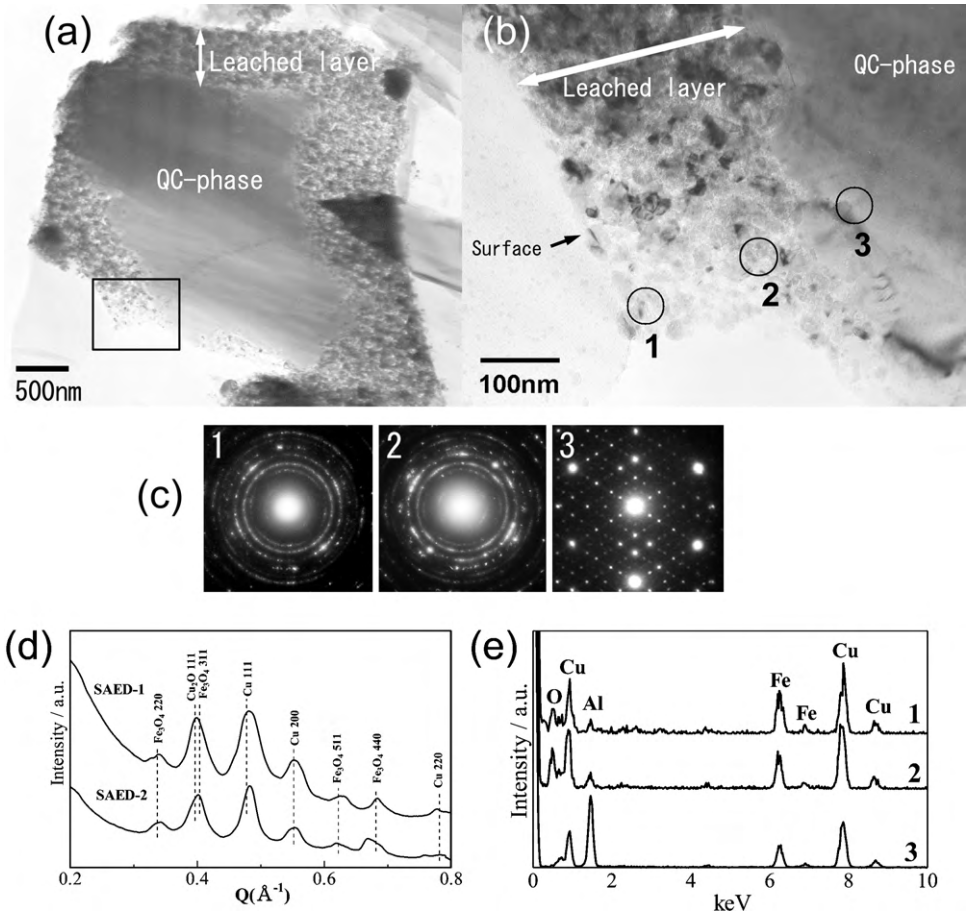

Fig. 6. Cross-sectional bright field image of fresh quasicrystalline $Al_{63}Cu_{25}Fe_{12}$ alloy catalyst (QC-AlCuFe) (a). The rectangular inset in Fig. 6(a) is enlarged and shown in Fig. 6(b). SAED patterns (c), line profiles of the SAED patterns (d), and EDS spectra (e). The SAED patterns and EDS spectra were obtained from the circled regions (1–3) in Fig. 6(b).

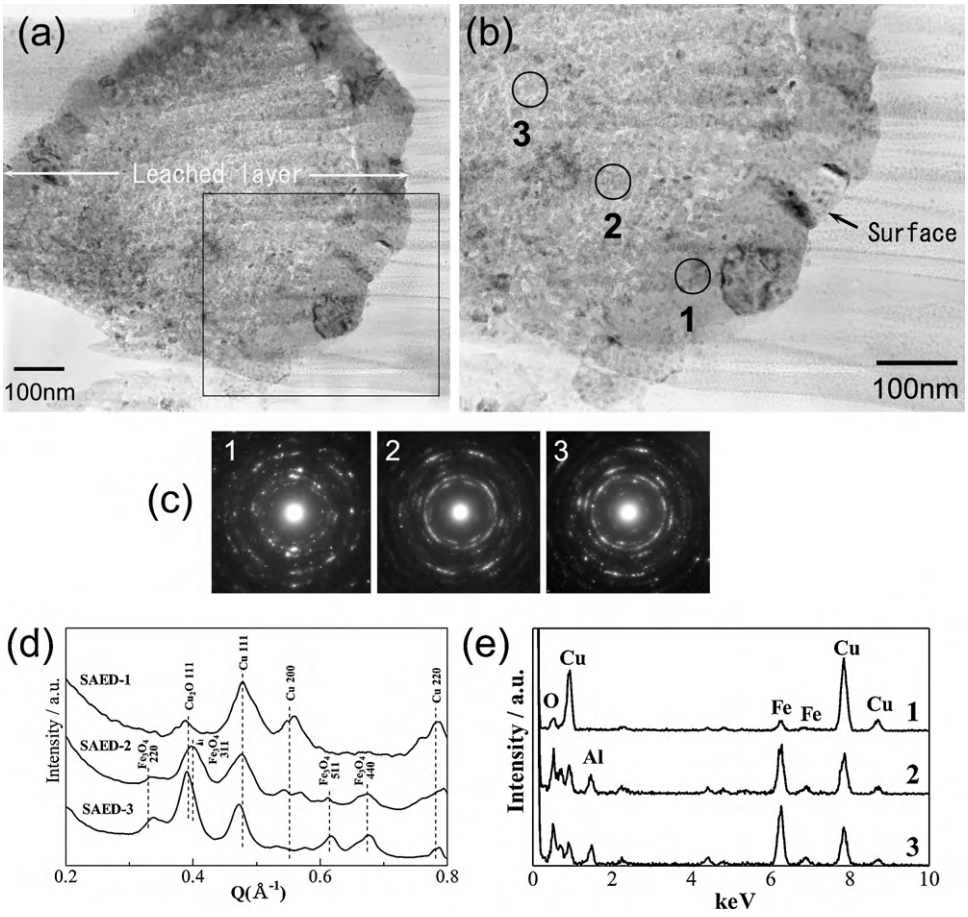

Fig. 7. Cross-sectional bright field image of fresh crystalline $Al_{70}Cu_{20}Fe_{10}$ alloy catalyst (C-AlCuFe) (a). The rectangular inset in (a) is enlarged and shown in (b). SAED patterns (c), line profiles of the SAED patterns (d), and EDS spectra (e). The SAED patterns and EDS spectra were obtained from the circled regions (1–3) in (b).

the addition of FeO_x to Cu/Al_2O_3 leads to the formation of highly dispersed Cu. These reports support the results obtained by us. The other beneficial effect of Fe species is its enhancement of catalytic performance through the interaction between Cu and Fe oxide. It has been reported by several groups that the interaction between Cu and Fe oxide in Cu/FeO_x or supported Cu-Fe catalysts enhances catalytic activity and stability [30–38]. Recently, we have observed a unique orientation relationship of Cu to Fe_3O_4 where Cu took the same direction as Fe_3O_4 in reduced $CuFe_2O_4$ [39]. Eguchi et al. [35] have reported that lattice matching at the interface between Cu and Fe_3O_4 in reduced $CuFe_2O_4$. Okamoto et al. [31] reported that the direct interaction between Cu species and Fe oxide clusters could form new species to inhibit sintering and enhance catalytic activity. These reports indicate that the interface between Cu and Fe oxides is not solely a physical contact; the interface region is also the setting for certain chemical interaction. In this study, we have shown the origin of high activity and stability is due to the formation of homogenous mixture of Cu and Fe oxides in the leached layer of QC-AlCuFe. Moreover, as shown in Table 2, the ternary Al-Cu-Fe alloy catalysts (i.e., QC-AlCuFe and C-AlCuFe) showed higher TOF values than the binary Al-Cu alloy catalyst (C-AlCu) and Cu/ZnO. These results demonstrate that the Fe species in an Al-Cu-Fe alloy catalyst enhance the catalytic activity for the SRM. From these facts, we would infer that the interaction between Cu and Fe oxides in

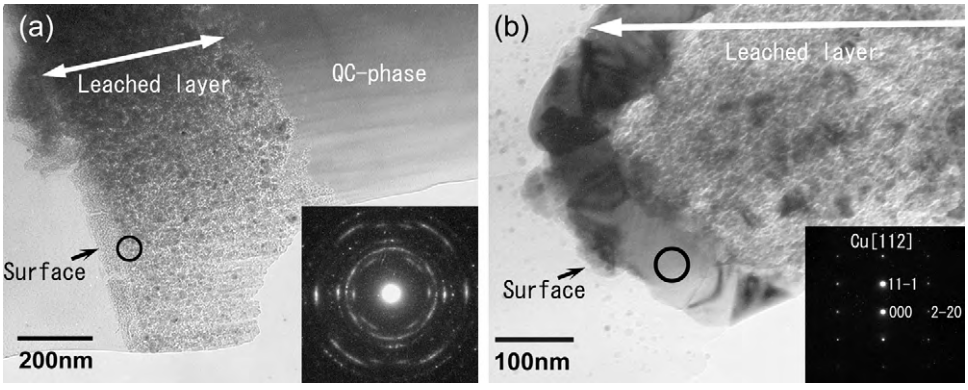

Fig. 8. Cross-sectional bright field images of spent quasicrystalline $Al_{63}Cu_{25}Fe_{12}$ alloy catalyst (QC-AlCuFe) (a) and crystalline $Al_{70}Cu_{20}Fe_{10}$ alloy catalyst (C-AlCuFe) (b). The SAED patterns were obtained from the circled regions in the figures.

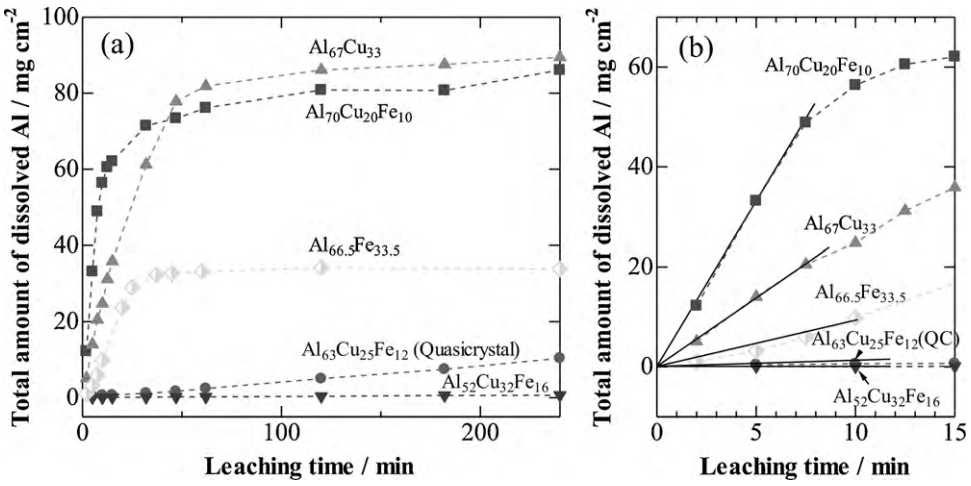

Fig. 9. Total dissolved Al into leaching solution as a function of leaching time for plate-type Al-Cu-Fe alloys (a). The beginning of the leaching process (up to 15 min) was shown in (b).

QC-AlCuFe stabilizes active Cu species and gives rise to the high catalytic performance for SRM. In spite of the inclusion of Fe, C-AlCuFe showed lower activity and stability compared to QC-AlCuFe. It is the formation of the Cu-layer at the edge (Fig. 7) that is responsible for this low catalytic performance. A lower amount of Fe in the Cu-layer (5 at.% Fe in region 1 in Fig. 7(b)) gives rise to a lower degree of contact and interaction between Cu and Fe species, as compared with the homogeneous leached layer of QC-AlCuFe (20 at.% Fe in region 1 in Fig. 6(b)). Thus, little beneficial effect is obtained from Fe species for C-AlCuFe. The origin of the difference in between the leached structures of QC-AlCuFe and C-AlCuFe will be discussed in Sections 3.4 and 3.5.

An other factor contributing to the high catalytic performance of QC-AlCuFe might be residual Al in the leached layer. EDS measurements of QC-AlCuFe (Fig. 6(e)) showed a small amount of residual Al in the homogeneous leached layer (10 at.% Al in region 1 in Fig. 6(b)). On the other hand, a rare amount of residual Al (<1 at.% Al in region 1 in Fig. 7(b)) was detected in the Cu-layer of C-AlCuFe (Fig. 7(e)), where the sintering of Cu developed during the SRM (Fig. 8(b)). This suggests the possibility that the residual Al contributed to the enhancement of catalytic performance, even as no beneficial effects of residual Al were observed for Raney Cu catalyst [40,41]. Therefore, the role of residual Al remains unclear at this stage.

3.4. Formation mechanism of leached layer

The formation mechanism of the leached layer of the Al-Cu-Fe alloy catalysts was examined by an Al-dissolution test for the plate-type Al-Cu-Fe alloys. Fig. 9(a and b) shows the total amount of Al that was dissolved into the leaching solution during the leaching time. At the beginning of the leaching process (up to 15 min of the leaching time), the dissolution of Al increased linearly with respect to the leaching time, as shown in Fig. 9(b), then subsequently slowed down. The linear regions were used to derive the apparent dissolution rate of Al from the Al-Cu-Fe alloys. Fig. 10 shows the relationship between the dissolution rate of Al and the Al content of the Al-Cu-Fe alloys. The dissolution rate of Al showed an approximately logarithmic increase with respect to the Al content i.e., the dissolution rate of Al has a linear relationship to the Al content. Overall, the leaching process is dominated by the Al content of the Al-Cu-Fe alloy, but this is not the case for the QC alloy ($Al_{63}Cu_{25}Fe_{12}$), whose dissolution rate deviates from a linear relationship, and is considerably lower than the predicted dissolution rate with respect to Al content.

Fig. 11(a–c) shows cross-sectional SEM images of the area around the interface between the leached and unleached regions of plate-type alloys. Their compositions, as determined by an EDS from the points indicated in Fig. 11(a–c), are also shown in Fig. 11(d–f), respectively. QC-AlCuFe(plate) (leached plate-type QC alloy) shows that the entire leached region formed on the unleached bulk consists of a homogenous mixture of Cu, Fe, Al, and their oxide particles, with thin leaf-shaped precipitates of Al oxides on top of the leached region (Fig. 11(a and d)). For C-AlCuFe(plate), the leached area was a complicated structure. Adjacent to the leached–unleached interface was a mixture of Cu, Fe, Al, and their oxide particles, with is a skeletal (or network) Cu structure on top of it (Fig. 11(b and e)). On C-AlCu(plate), only a very fine skeletal structure consisting of Cu was formed over the entire leached region (Fig. 11(c and f)).

SEM observation showed that the skeletal Cu structure was found in C-AlCuFe(plate) and C-AlCu(plate), while the only homogenous granular products were formed on QC-AlCuFe(palte). The difference in the microstructures of the leached QC and crystalline alloys is interpreted in terms of the dissolution rates of Al upon leaching. The dissolution rate of Al (Fig. 10) showed that the dissolution rate from the QC alloy (4×10^{-2} mg Al/cm^2/min) is much lower than the dissolution rate from the crystalline $Al_{70}Cu_{20}Fe_{10}$ (7 mg Al/cm^2/min) and $Al_{67}Cu_{33}$ (2 mg Al/cm^2/min) alloys. This result suggests that the low dissolution rate of Al from the QC alloy induces the formation a homogeneous mixture of

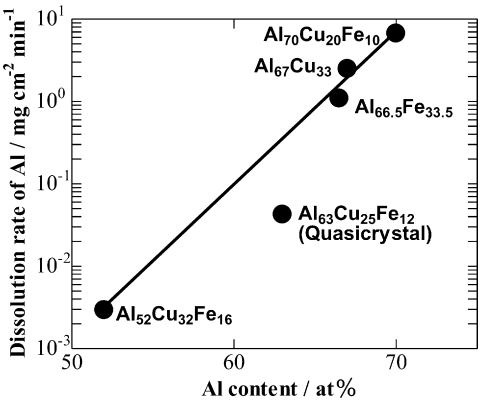

Fig. 10. Relationship between the dissolution rate of Al and the Al content of Al-Cu-Fe alloys. The dissolution rates of Al were estimated from the slopes of the liner regions in Fig. 9(b).

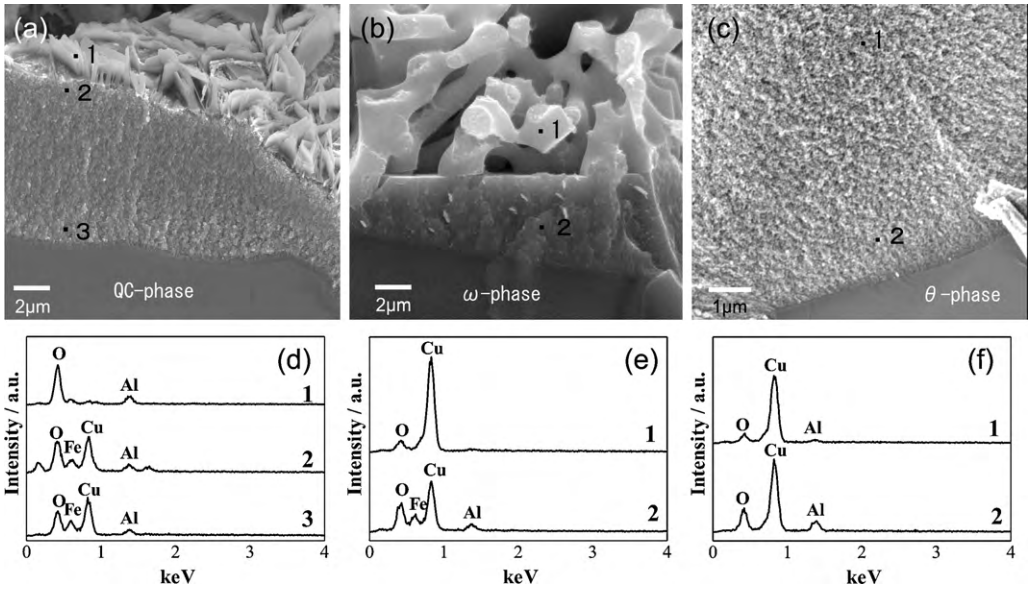

Fig. 11. Cross-sectional SEM images of the area around interface between the leached and unleached regions of leached plate-type quasicrystalline $Al_{63}Cu_{25}Fe_{12}$ alloy (QC-AlCuFe(plate)) (a), crystalline $Al_{70}Cu_{20}Fe_{10}$ alloy (C-AlCuFe(plate)) (b), and crystalline $Al_{67}Cu_{33}$ alloy (C-AlCu(plate)) (c). EDS spectra (d-f) were obtained from the points indicated in (a–c), respectively.

residual components (i.e., Cu, Fe, and Al) over the entire leached region, as shown in Fig. 11(a). It is likely that the homogeneous leached region is generated by the smooth precipitation of Cu and Fe following a slow Al-dissolution upon leaching. On the other hand, high dissolution rates from the crystalline alloys result in the formation of a skeletal Cu structure in the leached area (Fig. 11(b and c)). It may be suggested that the faster Al-dissolution induces a fluctuation in the concentration of Cu in the leached area, and that the Cu atoms are then chemically driven to aggregate into a skeletal structure through a phase separation process (spinodal-like decomposition). This process is similar to the dealloying of noble metal alloys in Al-Cu [22,42] and Ag-Au [43].

The observation of the leached-unleached interface of the plate-type alloys reveal the initial stage of the leaching process for QC and crystalline Al-Cu-Fe alloys, and the fully leached microstructure of the leached alloy has been identified by direct observation with a TEM (Figs. 6 and 7). According to these observations, a schematic illustration for the formation mechanism of the leached layer generated by the leaching of the QC alloy ($Al_{63}Cu_{25}Fe_{12}$) and crystalline alloy ($Al_{70}Cu_{20}Fe_{12}$) is proposed, and is shown in Fig. 12. In the case of the QC alloy, the homogeneous leached layer is generated from the start of the leaching, owing to the slow Al-dissolution. The reaction itself spontaneously stops at the point at which, the thickness of the homogeneous leached layer is about 500 nm and further leaching does not promote further change. The homogeneity of the leached layer is maintained even after the leaching treatment, as shown in the QC alloy catalyst (QC-AlCuFe) (Fig. 6). On the other hand, the fast Al-dissolution of the crystalline alloy ($Al_{70}Cu_{20}Fe_{10}$)

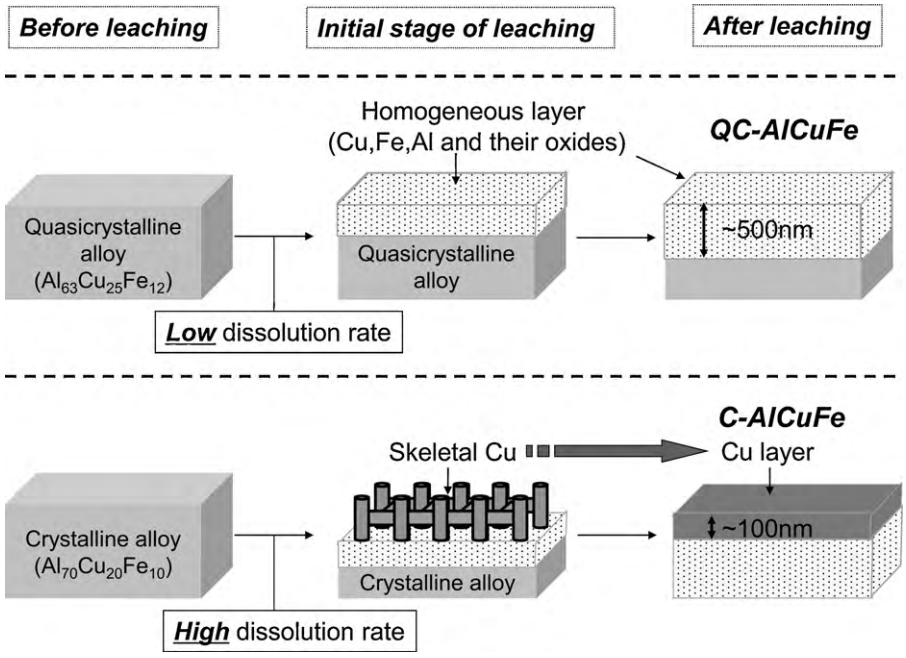

Fig. 12. Schematic formation mechanism of leached layer generated by the leaching of quasicrystalline $Al_{63}Cu_{25}Fe_{12}$ alloy and crystalline $Al_{70}Cu_{20}Fe_{10}$ alloy.

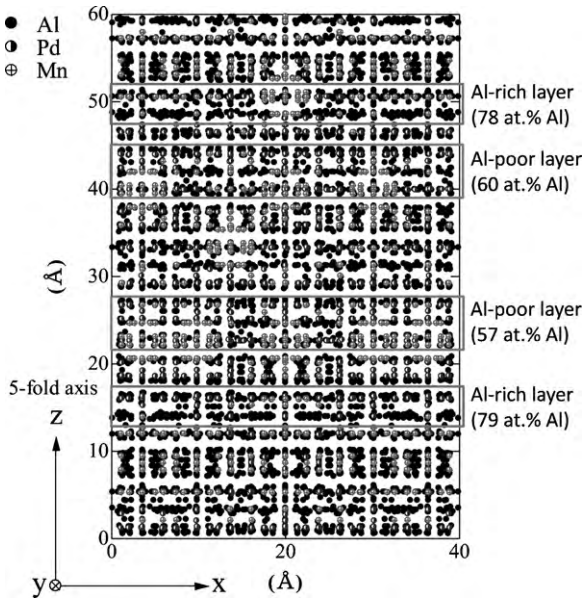

Fig. 13. Atomic position of the refined model structure of $Al_{71}Pd_{21}Mn_8$ quasicrystal [45] (isostructure of Al-Cu-Fe quasicrystal) projected normal to a 5-fold axis.

develops skeletal Cu at the initial stage of the leaching in consequence of a rapid phase separation process. Assisted by the exothermal reaction of the leaching and heavy stirring in the solution, the skeletal Cu aggregate is transformed into a Cu-enrichment region (Cu-layer) during the full leaching process. Consequently, the crystalline Al-Cu-Fe alloy catalyst (C-AlCuFe) possesses a Cu-layer at its edge.

3.5. Role of quasiperiodic structure

Al-dissolution test (Fig. 10) showed that the dissolution rate of Al was much lower for the QC alloy ($Al_{63}Cu_{25}Fe_{12}$) compared to the rate that was expected due to its Al content. The electrochemical behavior of an Al-Cu-Fe QC alloy in the same alkaline solution has been reported [44], with a corrosion rate of the Al-Cu-Fe QC alloy that is significantly lower than that of crystalline alloys; this finding supports our own results. We presume that the unusual dissolution behavior of the Al-Cu-Fe QC alloy is caused by its quasiperiodic structure. For the Al-Cu-Fe QC structure, the 5-fold planes are much more stable than other planes, as demonstrated by the frequent observations of pentagonal dodecahedral morphology [25]. Therefore, the dissolution rate on the 5-fold planes of the Al-Cu-Fe QC alloy dominates the leaching process. The recently refined model structure of an Al-Pd-Mn QC (isostructure of the Al-Cu-Fe QC) [45] showed that the bulk structure of the QC consists of atomically dense layers. The atomic position along a 5-fold axis of $Al_{71}Pd_{21}Mn_8$ QC is shown in Fig. 13. The model structure exhibits atomic dense layers of different composition, e.g., Al-rich dense layers whose composition contains more than ca. 80 at.% Al and Al-poor layers that contain less than ca. 60 at.% Al. There is a strong fluctuation in the concentration of Al along the 5-fold axes. This fluctuation of Al has been verified by several surface studies on the 5-fold planes of Al-Cu-Fe QC, whose surfaces always terminate at the layer with a high atomic density and Al contents of more than 80 at.% [3,46]. Since the concentration of Al dominates the leaching process of Al-Cu-Fe alloys, as shown in Al-dissolution test (Fig. 10), the leaching would be blocked on the layers with poor Al content in the Al-Cu-Fe QC structure and the overall dissolution rate would be slowed down. We suggest that the Al-Cu-Fe QC structure contributes to a decrease in the dissolution rate of Al for the QC phase. On the other hand, normal crystalline phases have a structure that is stacked by atomic planes having the same stoichiometry. Hence, there is less fluctuation of Al in crystal structures; therefore, the leaching proceeds smoothly and quickly.

4. Conclusions

In this paper, we have described the catalytic properties of the SRM, cross-sectional observation with TEM, and the leaching behavior of the Al-Cu-Fe alloy catalysts prepared by leaching with aqueous NaOH. This study demonstrates that the QC catalyst has a higher catalytic activity and durability than the related crystalline catalysts. The excellent performance of the QC catalyst is ascribed to the formation of a homogeneous leached layer that is generated by the leaching treatment. The dispersed Fe species in the homogeneous leached layer enhances the catalytic activity and suppresses the aggregation of Cu. The microstructure of the leached layer is predominantly controlled by the dissolution rate of Al upon leaching. The slow dissolution rate of Al from the QC structure produces a homogeneous leached layer with a high catalytic performance. The Al-Cu-Fe QC is an effective precursor for the fabrication of a high-performance catalyst via NaOH leaching.

Acknowledgements

The authors thank Mr. F. Sato for his technical assistance and received generous support from Prof. M. Terauchi of Tohoku University. This work was supported by Global COE Program "Materials Integration, Tohoku University," MEXT, Japan.

References

[1] D. Shechtman, I. Blech, D. Gratias, J.W. Cahn, Phys. Rev. Lett. 53 (1984) 1951–1953.
[2] A.P. Tsai, in: Z.M. Stadnik (Ed.), Physical Properties of Quasicrystals, Springer, Berlin, 1999, p. 5.
[3] H.R. Sharma, V. Fournee, M. Shimoda, A.R. Ross, T.A. Lograsso, A.P. Tsai, A. Yamamoto, Phys. Rev. Lett. 93 (2004) 165502.
[4] J. Hao, H. Cheng, H. Wang, S. Cai, F. Zhao, J. Mol. Catal. A: Chem. 271 (2007) 42–45.
[5] J.M. Hao, B.Z. Liu, H.Y. Cheng, Q. Wang, J.Y. Wang, S.X. Cai, F.Y. Zhao, Chem. Commun. (2009) 3460–3462.
[6] S.L. Chang, W.B. Chin, C.M. Zhang, C.J. Jenks, P.A. Thiel, Surf. Sci. 337 (1995) 135–146.
[7] P.J. Pinhero, S.L. Chang, J.W. Anderegg, P.A. Thiel, Philos. Mag. B 75 (1997) 271–281.
[8] M. Raney, US Patent 1 628 190 (1927).
[9] A.P. Tsai, M. Yoshimura, Appl. Catal. A 214 (2001) 237–241.
[10] M. Yoshimura, A.P. Tsai, J. Alloys Compd. 342 (2002) 451–454.
[11] S. Kameoka, T. Tanabe, A.P. Tsai, Catal. Today 93–95 (2004) 23–26.
[12] T. Tanabe, S. Kameoka, A.P. Tsai, Catal. Today 111 (2006) 153–157.
[13] B.P. Ngoc, C. Geantet, M. Aouine, G. Bergeret, S. Raffy, S. Marlin, Int. J. Hydrogen Energy 33 (2008) 1000–1007.
[14] J. Highfield, T. Liu, Y.S. Loo, B. Grushko, A. Borgna, Phys. Chem. Chem. Phys. 11 (2009) 1196–1208.
[15] B.P. Ngoc, C. Geantet, J.A. Dalmon, M. Aouine, G. Bergeret, P. Delichere, S. Raffy, S. Marlin, Catal. Lett. 131 (2009) 59–69.
[16] T. Tanabe, S. Kameoka, F. Sato, M. Terauchi, A.P. Tsai, Philos. Mag. (2007) 3103–3108.
[17] A.J. Smith, P.R. Munroe, T. Tran, M.S. Wainwright, J. Mater. Sci. 36 (2001) 3519–3524.
[18] P. Gallezot, P.J. Cerino, B. Blanc, G. Flehe, P. Fuertes, J. Catal. 146 (1994) 93–102.
[19] R. Wang, Z.L. Lu, T. Ko, J. Mater. Sci. 36 (2001) 5649–5657.
[20] C.B. Rodella, G. Kellermann, M.S.P. Francisco, M.H. Jordao, D. Zanchet, Ind. Eng. Chem. Res. 47 (2008) 8612–8618.
[21] A.D. Tomsett, D.J. Young, M.R. Stammbach, M.S. Wainwright, J. Mater. Sci. 25 (1990) 4106–4112.
[22] A.J. Smith, T. Tran, M.S. Wainwright, J. Appl. Electrochem. 29 (1999) 1085–1094.
[23] T. Fujitani, J. Nakamura, Catal. Lett. 56 (1998) 119–124.
[24] J.W. Evans, M.S. Wainwright, A.J. Bridgewater, D.J. Young, Appl. Catal. 7 (1983) 75–83.
[25] A.P. Tsai, A. Inoue, T. Masumoto, Jpn. J. Appl. Phys. 26 (1987) 1505–1507.
[26] M.V. Twigg, M.S. Spencer, Top. Catal. 22 (2003) 191–203.
[27] T.B. Massalski (Ed.), Binary Alloy Phase Diagrams, vol. 2, 2nd ed., AMS International, USA, 1990, p. 1408.
[28] Y. Kawamura, T. Ishida, W. Tezuka, A. Igarashi, Chem. Eng. Sci. 63 (2008) 5042–5047.

[29] H. Yahiro, K. Sagata, T. Yamamoto, K. Saiki, M. Asamoto, H. Yamaura, Catal. Lett. 124 (2008) 233–237.
[30] C.S. Chen, W.H. Cheng, S.S. Lin, Appl. Catal. A 257 (2004) 97–106.
[31] Y. Okamoto, T. Kubota, H. Gotoh, Y. Ohto, H. Aritani, T. Tanaka, S. Yoshida, J. Chem. Soc. Faraday Trans. 94 (1998) 3743–3752.
[32] S. Kameoka, T. Tanabe, A.P. Tsai, Catal. Lett. 100 (2005) 89–93.
[33] Y. Tanaka, R. Kikuchi, T. Takeguchi, K. Eguchi, Appl. Catal. B 57 (2005) 211–222.
[34] K. Faungnawakij, Y. Tanaka, N. Shimoda, T. Fukunaga, R. Kikuchi, K. Eguchi, Appl. Catal. B 74 (2007) 144–151.
[35] K. Eguchi, N. Shimoda, K. Faungnawakij, T. Matsui, R. Kikuchi, S. Kawashima, Appl. Catal. B 80 (2008) 156–167.
[36] K. Faungnawakij, T. Fukunaga, R. Kikuchi, K. Eguchi, J. Catal. 256 (2008) 37–44.
[37] K. Faungnawakij, N. Shimoda, T. Fukunaga, R. Kikuchi, K. Eguchi, Appl. Catal. A 341 (2008) 139–145.
[38] K. Faungnawakij, R. Kikuchi, T. Fukunaga, K. Eguchi, Catal. Today 138 (2008) 157–161.
[39] S. Kameoka, T. Tanabe, A.P. Tsai, Appl. Catal. A 375 (2010) 163–171.
[40] J.R. Mellor, N.J. Coville, A.C. Sofianos, R.G. Copperthwaite, Appl. Catal. A 164 (1997) 171–183.
[41] J.R. Mellor, N.J. Coville, A.C. Sofianos, R.G. Copperthwaite, Appl. Catal. A 164 (1997) 185–195.
[42] A.J. Smith, T. Tran, M.S. Wainwright, J. Appl. Electrochem. 30 (2000) 1103–1108.
[43] J. Erlebacher, M.J. Aziz, A. Karma, N. Dimitrov, K. Sieradzki, Nature 410 (2001) 450–453.
[44] A. Rudiger, U. Koster, in: E. Belin-Ferre, P.A. Thiel, A.P. Tsai, K. Urdan (Eds.), Quasicrystals-Preparation, Properties and Applications, Mater. Res. Soc. Symp. Proc., vol. 643, Boston, Massachusetts, 27–30 November, 2000, Warrendale, Pennsylvania, 2001, p. K2.3.1.
[45] A. Yamamoto, H. Takakura, A.P. Tsai, Phys. Rev. B 68 (2003) 094201.
[46] M. Gierer, M.A. Van Hove, A.I. Goldman, Z. Shen, S.L. Chang, C.J. Jenks, C.M. Zhang, P.A. Thiel, Phys. Rev. Lett. 78 (1997) 467–470.